

SEMI-ANNUAL REPORT

(for July - December 1994)

Contract Number NAS5-31363

OCEAN OBSERVATIONS WITH EOS/MODIS:

Algorithm Development and Post Launch Studies

Howard R. Gordon

University of Miami

Department of Physics

Coral Gables, FL 33124

(Submitted January 13, 1995)



Abstract

Several significant accomplishments were made during the present reporting period.

- Initial simulations to understand the applicability of the MODIS 1380 nm band for removing the effects of stratospheric aerosols and thin cirrus clouds were completed using a model for an aged volcanic aerosol. The results suggest that very simple procedures requiring no *a priori* knowledge of the optical properties of the stratospheric aerosol may be as effective as complex procedures requiring full knowledge of the aerosol properties, except the concentration which is estimated from the reflectance at 1380 nm. The limitations of this conclusion will be examined in the next reporting period.
- The lookup tables employed in the implementation of the atmospheric correction algorithm have been modified in several ways intended to improve the accuracy and/or speed of processing. These have been delivered to R. Evans for implementation into the MODIS prototype processing algorithm for testing.
- A method was developed for removal of the effects of the O₂ "A" absorption band from SeaWiFS band 7 (745–785 nm). This is important in that SeaWiFS imagery will be used as a test data set for the MODIS atmospheric correction algorithm over the oceans.
- Construction of a radiometer, and associated deployment boom, for studying the spectral reflectance of oceanic whitecaps at sea was completed. The system was successfully tested on a cruise off Hawaii on which whitecaps were plentiful during October–November. This data set is now under analysis.

1. Atmospheric Correction Algorithm Development

a. Task Objectives:

During CY 1994 there are five objectives under this task:

(i) Investigate the effects of stratospheric aerosol on the proposed correction algorithm, and investigate the possible use of the 1380 nm MODIS band to remove the stratospheric aerosol perturbation.

(ii) Investigate the effect of vertical structure in aerosol concentration and type. on the behavior of the proposed correction algorithm.

(iii) Investigate the effects of polarization on the accuracy of the algorithm.

(iv) Improve the accuracy and speed of the existing algorithm.

(v) Investigate removal of the O₂ "A" absorption band at 762 nm from the 745–785 nm SeaWiFS band so the latter can be used in atmospheric correction of SeaWiFS. The importance of this to MODIS is that SeaWiFS data will be used extensively to test and improve the MODIS algorithm. Thus, it is essential for the MODIS algorithm development and testing, that the O₂ absorption be adequately dealt with for SeaWiFS.

b. Work Accomplished:

(i) We have completed the addition of a third layer to our successive order of scattering radiative transfer code to include stratospheric aerosols. A literature search was carried out and three stratospheric aerosol models were selected representing a background stratospheric aerosol, a fresh volcanic aerosol, and an aged volcanic aerosol, Computations of the optical properties of the aerosol were carried out and initial radiative transfer simulations have been performed. The third layer in the model contains the stratospheric aerosol. To simulate the radiance observed in the 1380 nm band we use a single layer in our code and omit the Fresnel-reflecting sea surface.

This in effect assumes that all of the photons that penetrate through the stratospheric aerosol are immediately absorbed by water vapor in the free troposphere.

In the absence of stratospheric aerosol, the total reflectance at a wavelength λ , measured by MODIS can be decomposed as follows:

$$\rho_t(\lambda) = \rho_r(\lambda) + \rho_a(\lambda) + \rho_{ra}(\lambda) + t(\theta_v, \lambda)\rho_w(\lambda), \quad (1)$$

where $p_r(\lambda)$ is the radiance resulting from multiple scattering by air molecules (Rayleigh scattering) in the absence of aerosols, $p_a(\lambda)$ is the radiance resulting from multiple scattering by aerosols in the absence of the air, and $p_{ra}(\lambda)$ is the interaction term between molecular and aerosol scattering.¹ In this equation, t is the diffuse transmittance of the atmosphere along the viewing direction specified by θ_v , the angle between the normal to the sea surface and the sensor.² Radiance arising from specular reflection of direct sunlight from the sea surface (sun glitter) has been ignored because SeaWiFS can be tilted away from the glitter pattern. The influence of whitecaps has also been ignored under the assumption that their contribution can be removed from an estimate of the surface wind speed.³ The goal of the atmospheric correction is the retrieval of p_w from p_t .

The stratospheric aerosol contributes to the reflectance at all of the MODIS ocean bands. Thus, in the presence of the stratospheric aerosol layer the reflectance will be increased by an amount $\delta\rho_t^{(s)}$, i.e.,

$$\rho_t^{(s)}(\lambda) = \rho_t(\lambda) + \delta\rho_t^{(s)}(\lambda),$$

where $\rho_t^{(s)}$ is the reflectance of the entire ocean-atmosphere system in the presence of stratospheric aerosol. As much of this contribution as possible should be removed from the visible and NIR bands before applying the atmospheric correction. Thus, the goal is to be able to remove $\delta\rho_t^{(s)}(\lambda)$ from $\rho_t^{(s)}(\lambda)$ before applying the atmospheric correction algorithm, which was developed for application to $\rho_t(\lambda)$.

We have carried out simulations of radiative transfer with our three-layer model to examine several possibilities for utilizing the 1380 nm band for correction for stratospheric aerosols. Although, the analysis of these computations is incomplete, we will provide a brief report of the results thus far.

It is assumed that the reflectance at 1380 nm is totally due to the stratospheric aerosol. Also, as usual it is assumed that the aerosol properties in the lower layer are completely unknown. The atmospheric correction algorithm, as presently implemented, is then operated in several ways using the three-layer computations as pseudodata.

1. The "measured" reflectance at 443, 765 and 865 are used in the algorithm as usual, i.e., no attention is paid to the fact that a stratospheric aerosol may be present [$\rho_t^{(s)}(\lambda)$ assumed to be $\rho_t(\lambda)$], and the error in the atmospheric correction at 443 nm is determined.
2. The stratospheric aerosol is incorporated into the algorithm by simply subtracting the reflectance at 1380 nm from those at 443, 765, and 865, i.e., $\rho_t(\lambda) = \rho_t^{(s)}(\lambda) - \rho_t^{(s)}(1380)$, These are then inserted into the correction algorithm and determining the error in the correction at 443 nm is determined.
3. It is assumed that the spectral variation of the optical thickness of the stratospheric aerosol is known (either from an instrument like SAGE or from measurements from the surface), The reflectance at 1380 nm (due entirely to the stratospheric aerosol) is scaled by the ratio of the stratospheric optical depth at the given λ , $T_s(\lambda)$, to that at (or in the case of surface measurements, near) 1380 nm, and subtracted from the measured reflectance at the other wavelengths, i.e.,

$$\rho_t(\lambda) = \rho_t^{(s)}(\lambda) - \frac{\tau_s(\lambda)}{\tau_s(1380)} \rho_t^{(s)}(1380)$$

The $\rho_t(\lambda)$ are then inserted into the correction algorithm and the error in the correction at 443 nm determined.

4. It is assumed that accurate measurements or predictions of the other optical properties of the stratospheric aerosol, the spectral scattering phase function and single scattering albedo, along with the spectral variation of the optical depth are available for the stratospheric aerosol. The reflectance at 1380 nm is then scaled, by the ratio of the single-scattered stratospheric aerosol reflectance at λ to that at 1380 nm, and subtracted from the reflectance in the visible and NIR, i.e.,

$$\rho_t(\lambda) = \rho_t^{(s)}(\lambda) - \frac{\omega_s(\lambda)\tau_s(\lambda)p_s(\theta_v, \phi_v; \theta_0, \phi_0; \lambda)}{\omega_s(1380)\tau_s(1380)p_s(\theta_v, \phi_v; \theta_0, \phi_0; 1380)} \rho_t^{(s)}(1380),$$

where

$$p_s(\theta_v, \phi_v; \theta_0, \phi_0; \lambda) = P_s(\theta_-, \lambda) + \left(r(\theta_v) + r(\theta_0) \right) P_s(\theta_+, \lambda),$$

$$\cos \theta_{\pm} = \pm \cos \theta_0 \cos \theta_v - \sin \theta_0 \sin \theta_v \cos(\phi_v - \phi_0),$$

and $r(a)$ is the Fresnel reflectance of the interface for an incident angle a . The parameters $\tau_s(\lambda)$, $\omega_s(\lambda)$, and $P_s(\alpha, \lambda)$ are, respectively, the stratospheric aerosol optical thickness, single scattering albedo, and scattering phase function for a scattering angle α . The angles θ_0 and ϕ_0 are, respectively, the zenith and azimuth angles of a vector from the point on the sea surface under examination (pixel) to the sun, and likewise, θ_v and ϕ_v are the zenith and azimuth angles of a vector from the pixel to the sensor. These are measured with respect to the *upward* normal so θ_v and θ_0 are both less than 90° . The resulting values of $\rho_i(\lambda)$ are then inserted into the correction algorithm and the error at 443 nm is determined. This procedure is based on the assumption that the stratosphere aerosol enhancement of p_i is all due to single scattering.

5. As in (4) it is assumed that all of the optical properties of the aerosol are known except the concentration. A one-layer multiple scattering code (with a totally absorbing lower surface to represent the troposphere) is used to determine $\tau_s(1380)$ from $p_i^{(s)}(1380)$. This determines all of the optical properties of the stratospheric aerosol. These properties are inserted into a one-layer multiple scattering code (with a Fresnel-reflecting sea surface as the lower boundary) to compute $\delta\rho_i^{(s)}$, which is subtracted from the measured reflectance $\rho_i^{(s)}(\lambda)$ to provide $\rho_\tau(\lambda)$. The resulting values of are then inserted into the correction algorithm and the error at 443 nm is determined. This procedure is based on the assumption that there is no *radiative interaction* between the stratospheric aerosol layer and the other two layers.
6. Except for the step in which $\delta\rho_i^{(s)}(\lambda)$ is removed from $\rho_\tau(\lambda)$, this is identical to procedure 5. Once all of the optical properties of the stratospheric aerosol are known, they are inserted into a *two-layer* multiple scattering code (as opposed to a *one-layer* code in procedure 5 above) with a Fresnel-reflecting sea surface as the lower boundary. The top layer consists of the stratospheric aerosol and the lower layer has only Rayleigh scattering. This incorporates the Rayleigh-stratospheric aerosol interaction explicitly (albeit approximately because of the absence of the tropospheric aerosol), leaving only the Rayleigh-tropospheric aerosol and stratospheric-tropospheric aerosol interactions unaddressed. After subtracting the result of this computation from $\rho_i^{(s)}(\lambda)$, the result is inserted into the standard correction algorithm in which allowance is made for the fact that p_i has already been removed with the stratospheric component. This approach is possible because the properties of the Rayleigh scattering layer are completely known,

We now present the results obtained using these procedures for cases with an aged volcanic aerosol in the stratosphere with $\tau_s = 0.05$ and 0.15 , and a Maritime aerosol (relative humidity 80%) with $\tau_a = 0.15$ in the marine boundary layer. In the absence of stratospheric aerosol, the

algorithm yields an almost perfect atmospheric correction. Figures 1 and 2 provide the error in the recovered value of $tp_w(443)$ for each of the procedures above. On the figures the procedure number is given with the description of the symbols. The goal is that the error approach that which would be obtained were the stratospheric aerosol absent, which is provided by the very heavy black line. In the model description on the figures, the symbols "3L," "2L," "R," "S," and "(R+S)" stand for radiances computed from a three-layer model, a two-layer model, a one-layer model with Rayleigh scattering only, a one-layer model with stratospheric aerosol scattering only, and a two-layer model with stratospheric aerosols on the top and molecular scattering in the bottom.

To no surprise, the most complex method of dealing with the stratospheric aerosol (No. 6 above) yields the best overall correction; however, the second best methods (Nos. 1 and 2) are the simplest and require absolutely no *a priori* knowledge of the stratospheric aerosol's optical properties. This is similar the Gordon and Castaño⁴ conclusion regarding the influence of the El Chichon aerosol on CZCS atmospheric correction, i.e., that the presence of the aerosol had little effect on atmospheric correction.

(ii) A Monte Carlo code employing a fifty-layer atmosphere has been developed to carry out this investigation. To realistically treat the aerosol in the code, we divided the atmosphere into four broad regions: (1) the marine boundary layer from the surface to 2 km, where the aerosol concentration is independent of altitude; (2) the free troposphere, where the aerosol concentrations varies in proportion to $\exp[-z/h]$, where z is the altitude (2-12 km) and h (the scale height) is 2 km; (3) the background stratosphere (12-30 km), where the aerosol concentration is also exponential with a scale height of 5 km; and (4) a volcanic region (20-25 km) within the stratosphere which can contain a uniformly mixed volcanic aerosol. The optical properties of each of the four regions can be characterized by individual aerosol models, and any of the regions can be free of aerosols if desired.

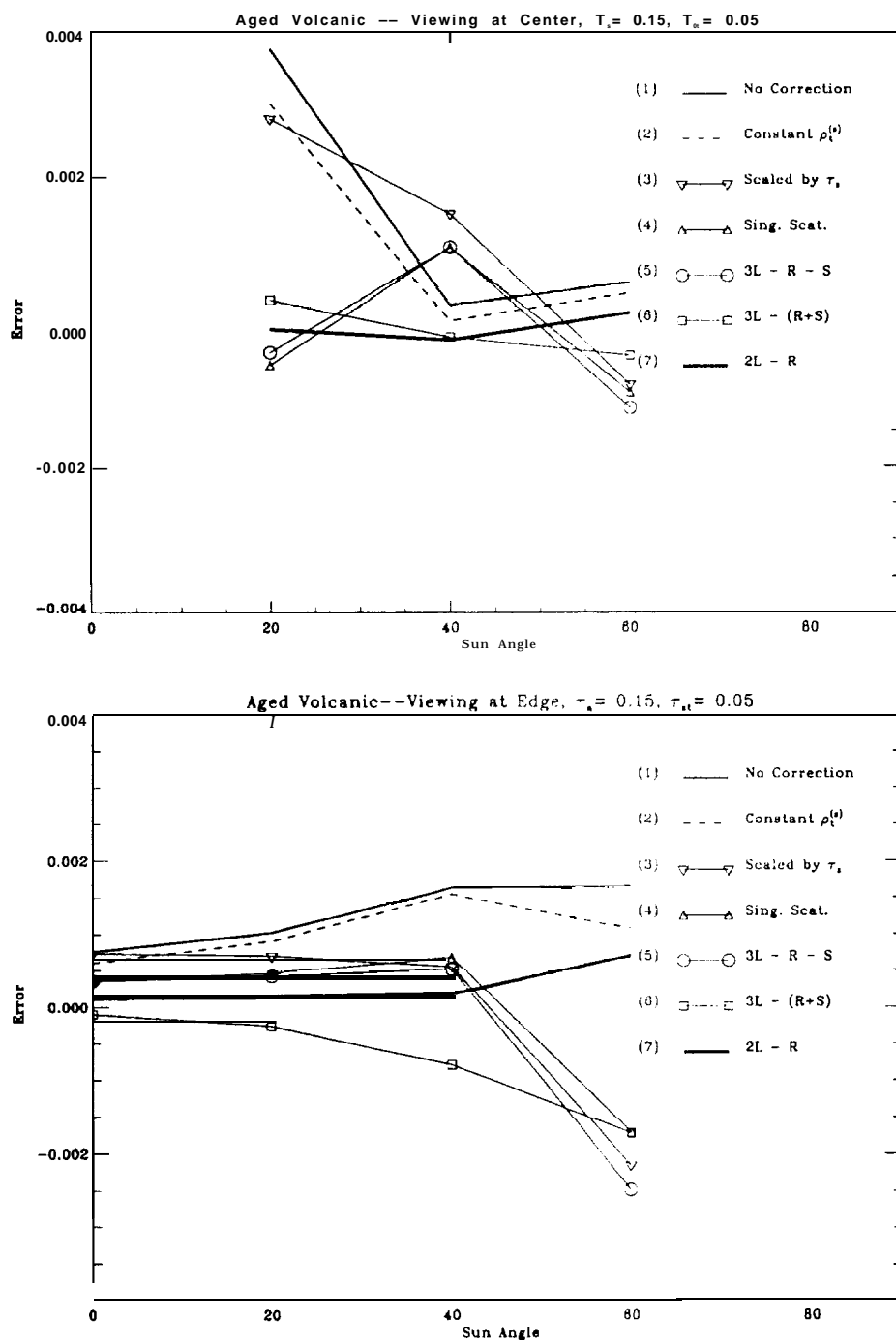


Figure 1. Error in retrieved water-leaving reflect ante as a function of the solar zenith angle for several methods of dealing with the stratospheric aerosol (1-6). $T_a = 0.15$, $T_{st} = 0.05$. Top: scan center, bottom: scan edge.

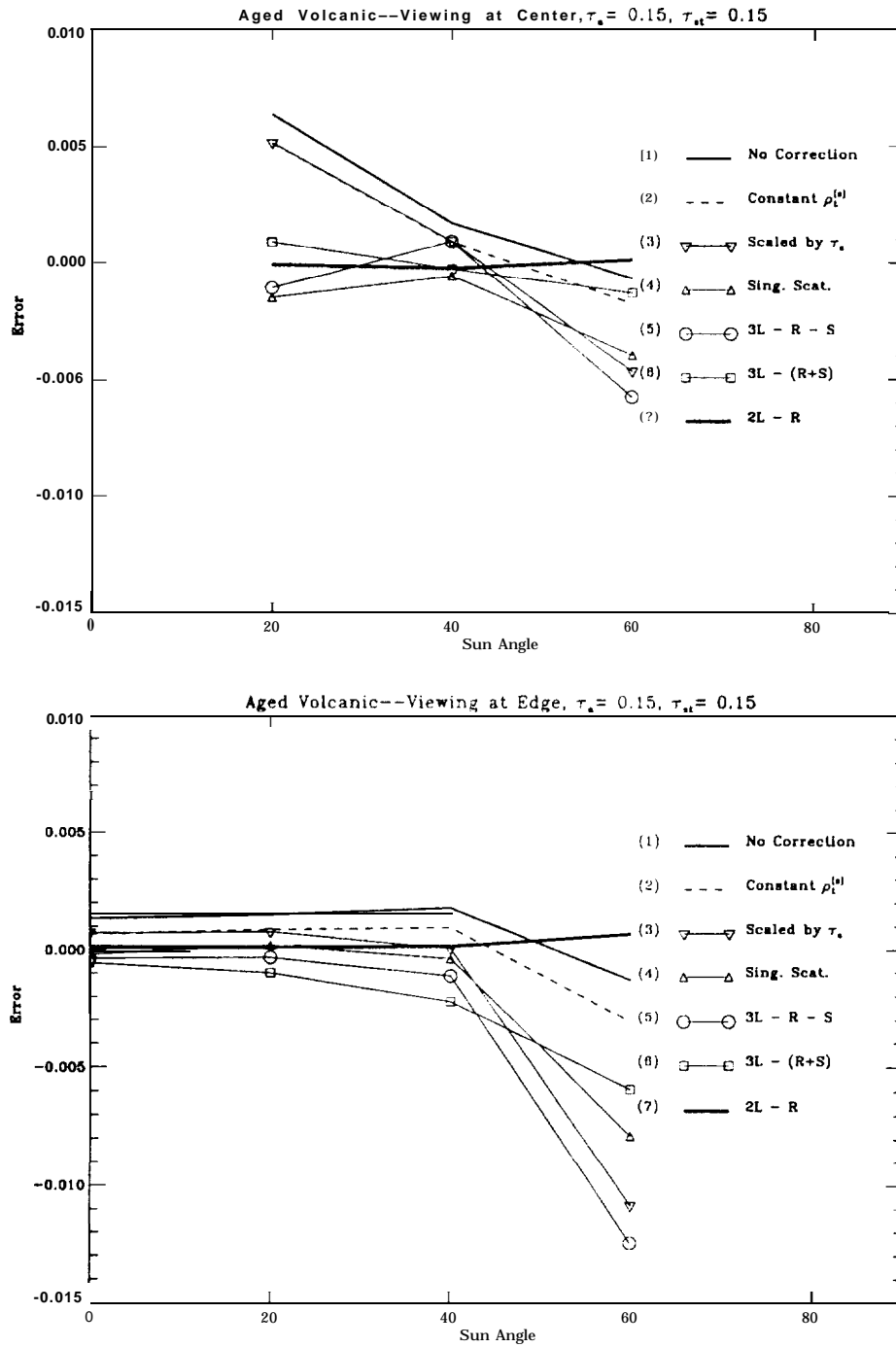


Figure 2. Error in retrieved water-leaving reflectance as a function of the solar zenith angle for several methods of dealing with the stratospheric aerosol (1-6). $\tau_a = 0.15$, $\tau_{st} = 0.15$. Top: scan center, bottom: scan edge.

The models for the two lower regions are taken from Shettle and Fenn.⁵ Briefly, based on size distribution and composition measurements they developed two models with log-normal size distributions called the Tropospheric (to model the aerosol in the free troposphere — few large particles) and the Oceanic (to model the aerosol produced by sea spray — few small particles). They combined these to form the Maritime model to represent the aerosol in the marine boundary layer. In terms of total aerosol number per unit volume the Maritime model consists of 99% Tropospheric and 1% Oceanic. Gordon and Wang⁶ added a Coastal model (99.5% Tropospheric and 0.5% Oceanic) to provide a description of the aerosol that might be more representative of the boundary layer near the coast.

For the two upper regions we use a model for the background stratosphere from the WMO⁷ and for the volcanic aerosol from King et al.⁸ Both models assume a 75% solution of H_2SO_4 . We have also included a volcanic ash model⁷ to represent fresh volcanic aerosol. The size distributions in these regions are modified gamma distributions.

The code contains provision for a wind-roughened sea surface with a surface slope distribution governed by the Cox and Munk⁹ probability density function.

Preliminary computations (using the code) relating to the influence of vertical structure of the aerosol on atmospheric correction (the algorithm assumes that the aerosol is all in the surface boundary layer) have been carried out. These show an increased error in the retrievals in the presence of vertical structure; however, the error is not excessive. We have not progressed further with this aspect of the study as we decided to complete the addition of polarization to the code first (the next item).

(iii) We have added polarization to our fifty-layer Monte Carlo code. Initial exercising of the code has been for an aerosol-free atmosphere. In this case the results agree with our successive order of scattering code¹⁰ to within ~ 0.1% for an atmosphere bounded by a flat Fresnel-reflecting ocean. For a sea surface roughened by the wind, differences in the two codes of the order of* 0.5% persist. Considerable effort on this part of the project during the last three months has been devoted to tracking down the source of this difference.

(iv) For the implementation of our correction algorithm,' extensive lookup tables relating $p_t - p_r - tp_w = p_a + p_{ra}$ to the single-scattered aerosol radiance, p_{as} , are required for each aerosol model we employ. Initially, we related $p_a + p_{ra}$ to p_{as} by

$$\log[\rho_t(\lambda) - \rho_r(\lambda) - t\rho_w(\lambda)] = \log[a(\lambda)] + b(\lambda) \log[\rho_{as}(\lambda)], \quad (2)$$

where $a(\lambda)$ and $b(\lambda)$ are the function of wavelength and the geometry. [For details, see the MODIS water-leaving radiance ATBD Version 2.] For a given aerosol model, we calculated the a and b from a linear fit of $\log(p_t - p_r - tp_w)$ to $\log(p_{as})$ for each wavelength and the given geometry, i.e., for all $\theta_v, \theta_0, \phi_v$ and λ , from simulations, using the method of least-squares. This resulted in a relationship that depends only on the aerosol model and geometry. It reduces the data storage of 3 ~ 4 times since the values of $p_t - p_r - tp_w$ and p_{as} need not be stored for each aerosol concentration, i.e., optical thickness (τ_a). For the angle ϕ_v , however, we still have to store $a(\lambda)$ and $b(\lambda)$ for a large number of values of the angle ϕ_v for interpolation. To further reduce storage, we expanded $a(\lambda)$ and $b(\lambda)$ in a Fourier series in ϕ_v and stored only the Fourier coefficients. All of the reflectance are even functions of the relative azimuth angle ϕ_v , so $p_t - p_r - tp_w$ and p_{as} are as well, and $a(\lambda)$ and $b(\lambda)$ will be even functions of ϕ_v . Thus, we can write

$$a(\theta_v, \theta_0, \lambda, \phi_v) = a^{(0)}(\theta_v, \theta_0, \lambda) + 2 \sum_{m=1}^M a^{(m)}(\theta_v, \theta_0, \lambda) \cos m\phi_v,$$

$$b(\theta_v, \theta_0, \lambda, \phi_v) = b^{(0)}(\theta_v, \theta_0, \lambda) + 2 \sum_{m=1}^M b^{(m)}(\theta_v, \theta_0, \lambda) \cos m\phi_v,$$

or

$$a^{(m)}(\theta_v, \theta_0, \lambda) = \frac{1}{\pi} \int_0^\pi a(\theta_v, \theta_0, \lambda, \phi_v) \cos m\phi_v d\phi_v,$$

$$b^{(m)}(\theta_v, \theta_0, \lambda) = \frac{1}{\pi} \int_0^\pi b(\theta_v, \theta_0, \lambda, \phi_v) \cos m\phi_v d\phi_v.$$

$a(\lambda)$ and $b(\lambda)$ for any ϕ_v can then be obtained easily from the stored values of $a^{(m)}$ and $b^{(m)}$. We have now investigated the use of azimuthal interpolation in place of the Fourier transform. This will increase the size of the tables; however, it may increase the speed. Also, to see if the accuracy of the lookup tables could be improved, we have also replaced Eq. (2) by

$$\log[\rho_t(\lambda) - \rho_r(\lambda) - t\rho_w(\lambda)] = \log[a(\lambda)] + b(\lambda) \log[\rho_{as}(\lambda)] + c(\lambda) \log^2[\rho_{as}(\lambda)]. \quad (3)$$

In the implementation of this using the Fourier transform, this increases the size of the lookup tables by 50%.

We have compared the accuracy of the atmospheric correction for standard test cases used in the MODIS water-leaving radiance ATBD, i.e., the Maritime, Coastal, and Tropospheric aerosol models with a relative humidity of 80%, $\tau_a = 0.2$ and 0.4 , solar zenith angles from $\theta_0 = 0$ to 60° , azimuth angle $\phi_v = 90^\circ$, and viewing angle $\theta_v = 45^\circ$ (scan edge). The scan center is not examined because the reflectance there is independent of ϕ_v . The results are presented in Tables 1-6. In the tables, the terms “linear” and “quad” refer to Eq. (2) and (3), respectively, the term “Fourier” refers to computations with 15 Fourier coefficients for a , b , and c (for the “quad” cases), and the numbers, 19, 24, and 37, refer to the number of values of ϕ_v used in the azimuthal interpolation. Noting that the maximum error in water-leaving reflectance at 443 nm is ± 0.001 – 0.002 , we note that there is little difference between the various schemes, with the exception that the quadratic fitting procedure [Eq. (3)] produces superior results for the Tropospheric cases with large τ_a . Thus, the choice probably should be based on the speed of the various algorithms.

(v) To simulate radiative transfer in the O_2 absorption, we modified our fifty-layer simulation code so that line-by-line computations could be carried out. What we wanted to learn was the influence of the O_2 absorption on the radiance or the reflectance leaving the top of the atmosphere (TOA) in a band extending from 745 to 785 nm (SeaWiFS band 7). Specifically, since the proposed SeaWiFS/MODIS algorithm ignores the O_2 absorption, our goal was to be able to estimate what the TOA radiance would be in the absence of the absorption band.

This study has been completed. Two simple modifications to the SeaWiFS algorithm suffice to correct for the absorption in the absence of stratospheric aerosols. A possible strategy for detecting stratospheric aerosols and/or thin cirrus clouds was also suggested. The complete study is included as Appendix 1. A paper describing the results is in press in *Applied Optics*.

c. Data/ Analysis/Interpretation: See item b above.

d. Anticipated Future Actions:

Table 1: Error in retrieved water leaving reflectance for viewing at edge through Tropospheric aerosols.
True value of $\tau_a(865)$ is 0.20.

Algorithm	θ_0			
	0°	20°	40°	60°
linear Fourier	+1.2787E-04	+1.8096E-04	+5.7206E-05	-1.5225E-03
linear 19	+1.2787E-04	+2.1100E-04	+1.3915E-04	-1.4221E-03
quad. Fourier	-9.9469E-05	-6.1776E-05	+1.7423E-05	+1.9481E-04
quad. linear 19	-9.9469E-05	-3.3934E-05	+1.0664E-04	+2.8400E-04
quad. linear 24	-9.9469E-05	-6.8206E-04	+2.8372E-05	+1.8390E-04
quad. linear 37	-9.9469E-05	-5.8398E-04	+4.6089E-05	+2.0859E-04

Table 2: Error in retrieved water leaving reflectance for viewing at edge through Coastal aerosols.
True value of $\tau_a(865)$ is 0.20.

Algorithm	θ_0			
	0°	20°	40°	60°
linear Fourier	+2.1622E-05	+1.8054E-04	+5.7206E-04	+1.6048E-03
linear 19	+2.1622E-05	+1.9103E-04	+5.9777E-04	+1.5984E-03
quad. Fourier	-1.4609E-04	-1.7202E-05	+2.9835E-04	+1.2792E-03
quad. linear 19	-1.4609E-04	-4.1556E-06	+3.2136E-05	+1.2924E-03
quad. linear 24	-1.4609E-04	-1.7000E-04	+2.8661E-04	+1.2534E-03
quad. linear 37	-1.4609E-04	-1.3556E-05	+2.9393E-04	+1.2632E-03

Table 3: Error in retrieved water leaving reflectance for viewing at edge through Maritime-aerosols.
True value of $\tau_a(865)$ is 0.20.

Algorithm	θ_0			
	0°	20°	40°	60°
linear Fourier	+6.4034E-05	+7.1921E-05	+5.9443E-05	-1.3646E-05
linear 19	+6.3950E-07	+7.5364E-05	+3.0333E-05	+7.6612E-05
quad. Fourier	-5.2648E-05	-8.7184E-05	-2.1609E-04	-3.5412E-04
quad. linear 19	-5.2648E-05	-7.2438E-05	-2.0611E-05	-3.1127E-04
quad. linear 24	-5.2648E-05	-8.8141E-05	-2.1783E-04	-3.6232E-04
quad. linear 37	-5.2648E-05	-8.6554E-05	-2.1681E-04	-3.5245E-04

Table 4: Error in retrieved water leaving reflectance for viewing at edge through Tropospheric aerosols. True value of $\tau_a(865)$ is 0.40.

Algorithm	θ_0			
	0°	20°	40°	60°
linear Fourier	-1.6432E-03	-2.0691E-03	-4.2873E-03	-1.1461E-02
linear 19	-1.6432E-03	-2.0169E-03	-4.1456E-03	-1.1328E-02
quad. Fourier	-1.1468E-03	-1.5905E-03	-3.4071E-03	-6.7699E-03
quad. linear 19	-1.1468E-03	-1.5418E-03	-3.2215E-03	-6.6015E-03
quad. linear 24	-1.1468E-03	-1.6033E-03	-3.3762E-03	-6.8075E-03
quad. linear 37	-1.1468E-03	-1.5905E-03	-3.3365E-03	-6.7561E-03

Table 5: Error in retrieved water leaving reflectance for viewing at edge through Coastal aerosols. True value of $\tau_a(865)$ is 0.40.

Algorithm	θ_0			
	0°	20°	40°	60°
linear Fourier	-1.4262E-04	+1.6253E-04	+7.5737E-04	+1.4211E-03
linear 19	-1.4262E-04	+1.8523E-04	+8.0941E-04	+1.4326E-03
quad. Fourier	-2.1960E-04	+2.9393E-06	+4.7064E-04	+1.5163E-03
quad. linear 19	-2.1960E-04	+2.1175E-05	+5.3098E-04	+1.5594E-03
quad. linear 24	-2.1960E-04	+5.6997E-07	+4.4502E-04	+1.4777E-03
quad. linear 37	-2.1960E-04	+6.9179E-06	+4.5546E-04	+1.4992E-03

Table 6: Error in retrieved water leaving reflectance for viewing at edge through Maritime aerosols. True value of $\tau_a(865)$ is 0.40.

Algorithm	θ_0			
	0°	20°	40°	60°
linear Fourier	-6.6683E-07	-4.5914E-05	-2.6444E-04	+3.8958E-04
linear 19	-8.4192E-07	-4.5866E-05	-8.9504E-05	-4.3686E-04
quad. Fourier	-3.7942E-05	-9.6641E-05	-1.6513E-04	+3.7413E-04
quad. linear 19	-3.7942E-05	-8.4076E-05	-7.0274E-05	+5.1993E-04
quad. linear 24	-3.7942E-05	-1.0493E-04	-1.2546E-04	+4.6471E-04
quad. linear 37	-3.7942E-05	-1.0111E-04	-1.1231E-04	+4.7841E-04

(i) We will continue our analysis of the existing simulations from the three-layer code to try to understand how to utilize the 1380 nm MODIS band to eliminate the influence of stratospheric aerosol. New simulations will be carried out for a variety of stratospheric aerosol types and amounts to understand the limits of our conclusions described in Section 1 b.(i).

(ii) We will exercise our fifty-layer MODIS simulation code to provide a better understanding of the influence of the aerosol's vertical profile (in concentration and in type) on the reflectance at the top of the atmosphere. In this way we will determine the required inputs into the three-layer radiative transfer code for the preparation of atmospheric correction lookup tables. This will start when we complete the addition of polarization to the code.

(iii) We will complete work on the addition of polarization to our MODIS simulation radiative transfer code. Our goal is to have a validated code during the first quarter of 1995.

(iv) We have supplied R. Evans with a new set of lookup tables and access subroutines to see the effect of azimuthal interpolation (as opposed to Fourier transformation) on the operation of the SeaWiFS — the MODIS prototype — atmospheric correction code. This completes our part of the this objective.

(v) Objective completed.

e. Problems/Corrective Actions:

(i) None.

(ii) Our initial simulations using the MODIS simulation code suggests that a single set of lookup tables based on an assumed simple vertical profile for the aerosol may not be sufficient to process the data. For example, African dust carried over the Tropical Atlantic is not in the boundary layer as assumed in the lookup tables; a separate set of tables must be used to deal with such situations. Similar problems arise from the presence of strongly absorbing aerosols, which are not in the basic set of models utilized in the present tables, and from the presence of volcanic aerosol in the stratosphere, which are absent as well. Thus, the inescapable conclusion is that the

lookup tables will have to be regenerated many times using different assumptions in order to be prepared to deal with most of the scenarios known to exist.

Regeneration of the lookup tables is a formidable task. The individual simulations require approximately 10 minutes on the DEC 3000/400. Thus, 33,000 simulations would require approximately 5500 hours, or approximately 230 days (7.5 months). Utilizing our original four CPU's on a 24-hour basis would reduce the computation time to about 2 months. This was unacceptable for many reasons. First if the computers are being used for routine lookup table generation no other research can be carried out. Next, the lookup tables will have to be regenerated many times not just once, so the computers would rarely be available for other aspects of the algorithm development. Finally, after launch of SeaWiFS and processing of the initial data is complete, we will be required to generate the necessary new sets of tables in a very timely manner, i.e., 1-2 weeks not several months. We decided we could meet this need with two DECserver 2100 systems, one of which was procured this year (1994) and with the remaining one scheduled for 1995.

The DECserver 2100 system has four processors each of which is approximately twice as fast as the DEC 3000/400 CPU. Thus, with one DECserver 2100 a single set of lookup tables could be generated in one month. With the addition of a second DECserver 2100, the generation time would be cut to two weeks, As we plan regular CPU upgrades of the DECservers, by the launch of MODIS the speed should be considerably faster which will also allow us to respond to unforeseen events in a timely manner. Under this plan the four existing DEC 3000/400 work stations will always be available for basic algorithm studies, as will the servers, when not generating tables. The DECserver 2100's will form the backbone of the Team Member's Computing Facility to be used for post-launch MODIS products.

(iii) None.

(iv) None.

(v) None.

f. Publications:

K. Ding and H.R. Gordon, Atmospheric correction of ocean color sensors: Effects of earth curvature, *Applied Optics*, 33, 7096-7016 (1994).

K. Ding and H.R. Gordon, Analysis of the influence of O₂ "A" band absorption on atmospheric correction of ocean color imagery, *Applied Optics* (In press).

M. Wang and H.R. Gordon, A Simple, Moderately Accurate, Atmospheric Correction Algorithm for SeaWiFS, *Remote Sensing of Environment* (In press).

2. Whitecap Correction Algorithm

a. Task Objectives:

As discussed in the previous report, our objective in this period was to build a new radiometer to measure the whitecap enhanced reflectance from the sea surface. This radiometer would be mounted on a boom off the bow of a ship, directed straight down. The radiometer would record the reflectance from a spot of the order of 10 cm in diameter on the sea surface in a continuous manner, and a video camera would be bore-sighted with this radiometer to help with data interpretation. The background return from clear water would provide the whitecap-free reflectance, and the reflectance above the background would provide the average reflectance enhancement of the ocean due to whitecaps. A self-contained meteorology package would determine the speed of the ship relative to the air, a GPS unit would provide the speed of the ship, and from the two the true wind vector would be recorded. Thus the reflectance increase as a function of the wind speed would be obtained for algorithm validation. We expected to be able to complete this instrument package by the end of the calendar year.

b. Work Accomplished:

During the past reporting period we built the whitecap radiometer and associated boom. The radiometer measured the upwelling radiance in six spectral bands (as opposed to the proposed three). These bands were spread throughout the visible from 410 nm to 860 nm (410 nm, 500 nm, 550 nm, 670 nm, 760 nm, 860 nm). This system was field tested during a three week MODIS cruise

off of Hawaii (R/V Mauna Wave, Chief Scientist Dennis Clark), and the radiometer performed very well. To convert the upwelling radiance into reflectance, downwelling irradiance was obtained with an old instrument that we had available (5 channel deck cell). This instrument did not perform as well, and needs to be updated. Because of some delays we were not able to obtain the bore-sighted video camera or meteorology station. Fortunately in all these cases redundant data was available from other cruise participants. Weather records were recorded by Dr. Stan Hooker and Mr. Jim Brown, a video camera was borrowed for short periods from Dennis Clark, and we did side by side irradiance measurements with another deck cell operated by Dennis Clark. With all of these measurements a very good initial trial data set was obtained. We are currently reducing this data, with particular attention to getting correct irradiance measurements for accurate reflectance values.

c. Data/ Analysis/Interpretation:

During the cruise mentioned in the previous section a good data set for whitecaps was obtained. The wind was typically 20 knots almost every day, with plenty of whitecaps visible. We are currently reducing this data.

d. Anticipated Future Actions:

The following improvements or augmentations to the system will be performed in the next 6 month period.

1. A video system will be obtained and added to the system to allow easier data interpretation. During the sea test of the instrumentation it was obvious that this is an important addition to the system.
2. The five channel deck cell will be rebuilt to increase the data to 6 channels, and to correct some of the stability and reliability problems experienced during the field test.
3. The meteorology package will be integrated into the system.

4. The system will be field tested on cruises in which we participate.

Other actions are to work and complete the data reduction for the initial data set which we have already collected.

e. Problems/Corrective Actions: See item d above.

f. Publications:

H.R. Gordon and M. Wang, Influence of Oceanic Whitecaps on Atmospheric Correction of SeaWiFS, *Applied Optics*, 33, 7754-7763 (1994).

3. In-water Radiance Distribution.

a. Task Objectives:

Acquire radiance data at sea.

b. Work Accomplished:

Radiance camera is now basically complete.

c. Data/ Analysis/Interpretation: None.

d. Anticipated Future Actions:

Acquire data at sea at the earliest opportunity. This will most likely be cruises scheduled by Dennis Clark in July 1995 and Fall 1995.

e. Problems/Corrective Actions: None.

f. Publications: None.

4. Residual Instrument Polarization.

a. Task Objectives: None.

5. Direct Sun Glint Correction.

a. **Task Objectives:** None.

6. Prelaunch Atmospheric Correction Validation.

a. **Task Objectives:**

The long-term objectives of this task are two fold. First, we need to demonstrate that our atmospheric correction scheme will work to the required accuracy. To effect this we will apply the algorithm to compute the sky radiance in the blue from measurements in the near infrared. We should be able to do this to about the same accuracy as looking downward from space. Second, we need to study the properties of aerosols over the ocean, in particular the aerosol phase function and its spectral variation, in order to verify the applicability of the aerosol models on which we are basing the atmospheric correction.

To carry out these objectives requires instrumentation for measuring the sky radiance, solar aureole, and the optical thickness of the atmosphere. Instrumentation for measuring the optical thickness and the sky radiance is available in our laboratory and has been modified to operate with the relevant MODIS spectral bands. Development of an aureole camera for use on a ship is a high priority because the sky radiance near the sun is required in aerosol optical property retrieval algorithms. Our near-term objective was to see if such inversions could be carried out without aureole data. A second objective was to develop and assemble an aureole camera system for obtaining such data at sea. The third objective is to begin to obtain a long-term time series of the aerosol properties in a maritime environment. For this we are in the process of procuring a CIMEL sun/sky radiometer that can be operated in a remote environment and send data back to the laboratory via a satellite link. These are similar to the radiometers used by B. Holben and Y. Kaufman.

b. Work Accomplished:

We planned and executed a field trip to Key West, FL in April (1994) to obtain sky radiance and other aerosol data. Key West is a small island and was chosen to simulate as much as possible measurements made from a ship, i.e., to reduce the perturbation by the land as much as possible. The planned measurements included (1) aerosol optical thickness as a function of wavelength in nine bands from 380 to 1026 nm, (2) sky radiance using the full-sky camera at 560, 671, and 860 nm, and (3) sky radiance at selected positions using a hand-held radiometer at 558, 669, and 866 nm. We began analysis of the Key West data; however, for the only day with a clear enough sky, the data were obtained at such a small solar zenith angle that inversion is only accurate for the forward part of the phase function. Our present inversions yield a value of single scatter albedo that was far too low. We are trying to track down the source of the difficulty; however, we believe that the error results from the absence of solar aureole data.

The aureole camera system has now been designed and assembled. The idea is fairly simple, a cooled CCD camera has been outfitted with a lens focused at infinity, an interference filter which selects the spectral band of interest, and a small aperture over this filter. A neutral density occulter is placed approximately 1 meter from the aperture, and this occulter is positioned to block the direct sunlight from entering the camera system. In this manner the sky radiance close to the sun can be measured, without the direct sunlight (approximately 6 orders of magnitude larger) interfering with the measurement. We are currently doing the characterization of the camera system electronics and optics. This is part of the calibration procedure. During the next reporting period we will also be assembling the field data acquisition software package. Our goal is to field test this system during a short cruise in July.

The CIMEL Electronique, Automatic Sun Tracking Photometer, a Vitel Inc. GOES Data Transmitter with accessories, and a set of Solar Power Panels are now on order.

c. Data/ Analysis/Interpretation: Nothing concrete yet.

d. Anticipated Future Actions:

During the next reporting period we will be working on characterizing the camera system, and finalizing the data acquisition software. We had also expected to participate on a short cruise off of Hawaii during February on which we could have tested this system at sea and acquired a more complete sky radiance data set. The cruise track for this cruise was optimal for us as it was planned to stay in the lee of Lanai, an area where cloud free skies are probable. Due to the slip in the SeaWiFS launch, this cruise has now been rescheduled for July.

We also expect to take delivery of the CIMEL Electronique, Automatic Sun Tracking Photometer and assemble to radiometer with the GOES Data Transmitter and Solar Power Panels. Testing will begin after assembly with the goal of deploying the instrument in the field in the first six months of 1995.

e. Problems/Corrective Actions: None.

f. **Publications:** None.

7. Detached Coccolith Algorithm and Post Launch Studies.

a. Task Objectives:

The algorithm for retrieval of the detached coccolith concentration from the coccolithophorid, *E. huxleyi* is described in detail in our ATBD. The key is quantification of the backscattering coefficient of the detached coccolith. Our earlier studies showed that calcite-specific backscatter coefficient was less variable than coccolith-specific backscatter coefficient, and this would be more scientifically meaningful for future science that will be performed with this algorithm. The variance of the calcite-specific backscatter has been analyzed for only a few species, thus, we need to examine this in other laboratory cultures and field samples. There is also a relationship between the rate of growth of the calcifying algae and the rate of production and detachment of the coccolith which needs to be further quantified. With this in mind, the objectives of our coccolith studies are, under conditions of controlled growth of coccolithophore (using chemostats), to define the effect of growth rate on:

- the rate that coccolith detach from cells (which also is a function of turbulence and physical shear);
- the rates of coccolith production;
- the morphology of coccolith; and
- the volume scattering and backscatter of coccolith.

The last aspect of these studies will be to perform shipboard measurements of suspended calcite and estimate its optical backscatter as validation of the laboratory measurements. A thorough understanding of these growth-related properties will provide the basis for a generic suspended calcite algorithm. As with algorithms for chlorophyll, and primary productivity, the natural variance between growth related parameters and optical properties needs to be understood before the accuracy of the algorithm can be determined.

b. Work Accomplished:

In the last 6 months, we have performed experiments on the effect of turbulence on the rate of detachment of coccolith. These studies were performed under highly controlled conditions of turbulent dissipation rates. The rationale for this work was that in order to grow these organisms, they must be stirred and since one of our goals is to relate coccolith detachment to growth rate, we must insure that we understand the independent effects of turbulence on detachment.

For the studies of coccolith morphology, we have recently modified our microscope system with a phase contrast optical system which gives us much more resolution than we have ever had. This will save us considerable time in estimating numbers and morphologies of coccolith because before, we needed to use a scanning electron microscope and make measurements on dead specimens. Now, we can count coccolith and check morphology on living specimens using light microscopy (which is essentially instantaneous). In fact, we can actually count the numbers of these 2 micrometer diameter plates on individual cells.

Successful algorithm development also requires sea-truth data. We continued our analyses of optical data from a coccolithophore bloom in the North Atlantic. These data include volume scatter measurements, absorption measurements, pigment measurements, cell counts, suspended calcite measurements and particulate organic carbon and nitrogen measurements. The first paper on this material has been submitted for publication.

c. Data/Analysis /Interpretation:

Our results from the laboratory experiments showed that when the cells are actively growing, coccolith detachment is not a function of turbulence. However, when cell growth slows or stops, then plates are held more loosely such that turbulence and coccolith detachment are directly related. This represents the first physiological study directly relating turbulence to detachment of coccolith.

In regards to our work-up of scatter and absorption data from a coccolithophore bloom in the north Atlantic, we have found that chlorophyll-specific absorption by field populations of *E. huxleyi* was similar to previously reported laboratory culture measurements of the same species. Volume scatter measurements showed that the suspended coccolith were responsible for about 80% of the total backscatter, b_b , in the center of the bloom. Vertical profiles of backscatter showed that greatest calcite-dependent light scatter was observed just below the base of the mixed layer. Areal maps of calcite-dependent backscatter and reflectance (calculated from absorption and backscatter) were extremely similar, due to the dominance of backscatter over absorption. Calculated reflectance in this mesoscale feature reached as high as 21% at 440 nm and 24% at 550 nm, slightly less than what has been observed previously in Gulf of Maine blooms. Total scatter, b , was also calculated as the difference between beam attenuation and absorption. The ratio of backscatter to total scatter $\tilde{b}_b \equiv b_b/b$ was about 0.01-0.02 at 440 nm and 550 nm for b values of 1 to 3 m^{-1} . As total scatter decreased from 1 m^{-1} , b_b increased. The behavior of b_b is compared for coccolith-dominated versus chlorophyll-dominated waters. Vertical profiles of calcite-dependent scatter, combined with satellite remote sensing data, were used to assess the vertical transport velocity of coccolith (1-2 m per day). This velocity was an order of magnitude greater than that expected from theoretical Stokes sinking calculations and previous sinking rate experiments. A number of hypotheses are proposed

to explain the the discrepancy; the most likely of which is that the subsurface peak in calcite-dependent scatter did not result from detached coccolith sinking but resulted either from plated coccolithophore sinking, then detaching their plates, or from deep coccolithophore producing and detaching their plates in situ.

d. Anticipated Future Actions:

Given the completion of our turbulence experiments, we can now begin the chemostat experiments in which we will measure the light scatter properties of coccolithophore as a function of growth rate. These experiments should start in mid-February.

There is still more analysis to be done on the field coccolithophore data from the North Atlantic. There is sufficient material to publish a second paper on the relationship between backscatter, suspended calcite concentration, and reflectance. This will be written for *Limnology and Oceanography*.

e. Problems/Corrective Actions: None

f. Publications: None

8. Other Developments.

The PI spent a significant portion of the first quarter of this reporting period completing the necessary requests to obtain government permission to procure several items of capital equipment. Also, all personnel on the project devoted most of their effort in late September and October toward revising the Algorithm Theoretical Basis Document (ATBD) for normalized water leaving radiance. Version 2 of the ATBD's for Normalized water-leaving radiance (along with aerosol products) and detached coccolith were delivered to M. King on November 2, 1994.

The SeaWiFS/MODIS algorithm for estimating the aerosol optical thickness for has now been coded and will be delivered to R. Evans in January for incorporation into the processing system.

A method for combining high-altitude aircraft radiance (upwelling) and surface radiance (downwelling) for determination of the columnar aerosol optical properties has been developed. A paper

on the subject is nearly complete and will be submitted to *Applied Optics* in January. This could provide a powerful method of studying aerosol properties over the ocean. Also, a second study concerning the perturbation of the sky radiance measurements made from islands, caused by the presence of the island itself, has been carried out and a paper is in preparation. Both of these have relevance to the "Prelaunch Atmospheric Correction Validation" (Topic 6 above) portion of our research, as well as to the validation of retrieved aerosol properties over the oceans from EOS sensors.

9. References.

- [1] P. Y. Deschamps, M. Herman and D. Tanre, "Modeling of the atmospheric effects and its application to the remote sensing of ocean color," *Applied Optics* 22, 3751-3758 (1983).
- [2] H. R. Gordon, D. K. Clark, J. W. Brown, O. B. Brown, R. H. Evans and W. W. Broenkow, "Phytoplankton pigment concentrations in the Middle Atlantic Bight: comparison between ship determinations and Coastal Zone Color Scanner estimates," *Applied Optics* 22, 20-36 (1983).
- [3] M. Wang and H. R. Gordon, "Influence of Oceanic Whitecaps on Atmospheric Correction of SeaWiFS," *Applied Optics* 33, 7754-7763 (1994).
- [4] H. R. Gordon and D. J. Castano, "The Coastal Zone Color Scanner Atmospheric Correction Algorithm: Influence of El Chichon," *Applied Optics* 27, 3319-3321 (1988).
- [5] E. P. Shettle and R. W. Fenn, *Models for the Aerosols of the Lower Atmosphere and the Effects of Humidity Variations on Their Optical Properties* (Air Force Geophysics Laboratory, Hanscomb AFB, MA 01731, AFGL-TR-79-0214, 1979).
- [6] H. R. Gordon and M. Wang, "Retrieval of water-leaving radiance and aerosol optical thickness over the oceans with SeaWiFS: A preliminary algorithm," *Applied Optics* 33,443-452 (1994).

- [7] WCP-112, *A preliminary cloudless standard atmosphere for radiation computation* (World Meteorological Organization, WMO/TD-No. 24, Geneva, 1986).
- [8] M. D. King, Harshvardhan and A. Arking, "A Model of the Radiative Properties of the El Chichon Stratospheric Aerosol Layer," *Journal of Climate and Applied Meteorology* 23, 1121-1137 (1984).
- [9] C. Cox and W. Munk, "Measurements of the Roughness of the Sea Surface from Photographs of the Sun's Glitter," *Jour. Opt. Sot. of Am.* 44, 838-850 (1954).
- [10] H. R. Gordon and M. Wang, "Surface Roughness Considerations for Atmospheric Correction of Ocean Color Sensors. 1: The Rayleigh Scattering Component ," *Applied Optics* 31, 4247-4260 (1992).